A molecular dynamics study of sodium beta "-alumina

1992 J. Phys.: Condens. Matter 4 3215

(http://iopscience.iop.org/0953-8984/4/12/014)

J. Phys.: Condens. Matter 4 (1992) 3215–3234. Printed in the UK

A molecular dynamics study of sodium β''-alumina

W Smith† and M J Gillan‡

† Theory and Computational Science Division, SERC Daresbury Laboratory, Daresbury, Warrington, Cheshire WA4 4AD, UK

‡ Physics Department, University of Keele, Keele, Staffordshire ST5 5BG, UK

Received 30 October 1991

Abstract. The results of an extensive simulation study of non-stoichiometric sodium β''-alumina are presented. The simulations are performed using the molecular dynamics method on large periodic systems (3213 and 3204 ions) of differing stoichiometries at a series of temperatures between 200 and 1200 K. The simulated systems include all the ions in the spinel blocks, and are based on a realistic model for the interactions between the ions. The results presented give new insight into the dynamics of the diffusing ions, the non-Arrhenius behaviour of the ionic conductivity, the formation of the proposed vacancy superlattice, and the anomalous diffuse scattering observed in x-ray studies.

1. Introduction

The β- and β''-alumina compounds are an important class of solid electrolyte. Because of their technological and scientific significance, they have been widely studied, both experimentally and theoretically (see e.g. Bates and Farrington 1981, Kleitz *et al* 1983, Weppner and Schulz 1988, and references therein). Typical of the class is sodium β''-alumina, which has the general formula $Na_{2-x}Mg_{1-x}Al_{10+x}O_{17}$, where x is variable, but under normal preparation conditions is roughly 1/3 (Roth *et al* 1973). The material is thus non-stoichiometric, a fact which underlies its unusual physical properties. The work reported here is a theoretical study of sodium β''-alumina by the method of molecular dynamics (MD) simulation. There are two parts to this: firstly, we have studied in some detail the temperature dependence of the ionic electrical conductivity, which experimentally shows strong departures from Arrhenius behaviour. Secondly, we have investigated the vacancy superlattice which, according to x-ray scattering experiments, is spontaneously formed at temperatures below ~ 500 K. The work represents a significant advance on previous simulation work on the material, because the simulated systems we have studied are much larger, and the simulation runs much longer than those of previous workers.

The structure of the β''-alumina compounds is complex (Bettman and Peters 1969, Farrington and Briant 1979). They have a very large unit cell which consists of three spinel blocks containing aluminium, magnesium and oxygen ions. The spinel blocks are separated by planes in which the mobile ions (sodium in the present case) diffuse, the blocks on either side of each plane being linked by so-called bridging oxygen ions. The stoichiometric crystal, corresponding to $x = 0$, has the space group $R_{\bar{3}m}$, which implies hexagonal symmetry and a three-fold screw axis in the c-direction. The unit cell has lattice parameters $a = 5.614$ Å, $c = 33.85$ Å under ambient conditions,

0953-8984/92/123215+20$04.50

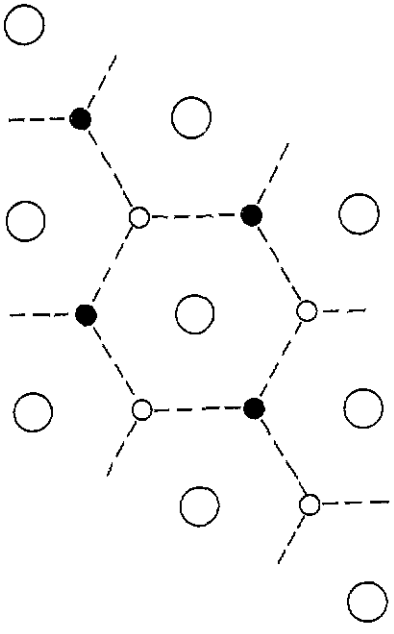

Figure 1. The conduction plane in stoichiometric sodium β''-alumina. The large circles represent bridging oxygens, which all lie in the same plane. The small black and white circles represent the occupied sodium sites.

and in the stoichiometric form contains 90 ions. As we shall describe below, our simulations are performed on systems containing 36 of these unit cells.

The structure of the conduction plane in which sodium diffuses is shown in figure 1. The regular lattice sites that can be occupied by sodium ions form a hexagonal network, every site being equivalent by symmetry. The unit cell contains two of these sites and one bridging oxygen in each conduction plane. The sodium sites do not all lie in a plane, but are displaced up and down along the c-axis by a small amount, which according to diffraction measurements is 0.17 Å (Bettman and Peters 1969). At the normally observed stoichiometry, corresponding to $x \simeq 1/3$, roughly one in every six sodium sites is vacant. The rapid diffusion of the vacancies gives rise to the well known liquid-like ionic conductivity of the material (Farrington and Briant 1979). In the work reported here, we are particularly interested in the effects of varying the stiochiometry, and we have performed simulations at values of x equal to 1/3 and 1/4, which correspond to vacancy concentrations of 1/6 and 1/8 respectively.

Two experimental properties of sodium β''-alumina are of particular interest here. Firstly, the DC electrical conductivity $\sigma(0)$ has a non-Arrhenius temperature dependence, the activation energy being considerably larger at low than at high temperatures. Conductivity measurements yield activation energies in the ranges 0.22–0.36 eV below 400 K and 0.03–0.09 eV above 600 K (Briant and Farrington 1980, Engstrom *et al* 1981). Secondly, x-ray diffuse scattering suggests that the vacancies in each conduction plane become ordered into a superlattice below $\sim$ 500 K (Boilot *et al* 1980). There appears to be a close connection between the non-Arrhenius behaviour of $\sigma(0)$ and the formation of the superlattice, since the change of Arrhenius slope also occurs in the region of 500 K. It has been suggested that pinning of vacancies by the superlattice may be responsible for the increased activation energy at low temperatures (Boilot *et al* 1980, Wang *et al* 1981, Bates *et al* 1981).

The present work enlarges on earlier molecular dynamics work on β''-alumina

by several workers including ourselves (Wolf *et al* 1984, Zendejas and Thomas 1988, Lane and Farrington 1991, Smith and Gillan 1991). The temperature dependence of $\sigma(0)$ has previously been studied by simulation in the work of Wolf *et al* (1984), though their simulated system was much smaller than those studied here, and their simulations were of much shorter duration. Their work was important because it demonstrated the possibility of making realistic simulations of materials as complex as β″-alumina, but because of the limited size of their system there was no possibility of observing superlattice formation; furthermore, the statistical accuracy of their results was not adequate to allow firm conclusions to be drawn about the temperature dependence of $\sigma(0)$. In later simulation work, Zendejas and Thomas (1988) and Lane and Farrington (1991) observed the formation of the vacancy superlattice in the $x = 1/3$ system, but did not study the phenomenon in any detail. We shall show in the present work that the ionic conductivity of our simulated material displays the non-Arrhenius behaviour observed experimentally, and also that spontaneous ordering of the vacancies into a superlattice occurs below the temperature at which the Arrhenius slope of the conductivity changes.

The remainder of this paper is organized as follows. In the next section, we describe the interionic potential model we have used, and give an overview of the simulations we have performed. Section 3 reports our results for the temperature dependent sodium diffusion coefficient and hence conductivity, and also summarizes briefly some results for the frequency spectrum of the sodium dynamics. Our observations on the formation of the vacancy superlattice at low temperatures in the $x = 1/4$ and $x = 1/3$ systems are presented in section 4. The study of the superlattice is continued in section 5, where we report results for the diffuse scattering intensity associated with vacancy ordering; here, we are able to make direct contact with the diffuse x-ray diffraction experiments of Boilot *et al* (1980). The paper ends with a summary of our conclusions, and some comments on problems that remain unresolved.

2. The simulations

In the present simulations, the interactions between the ions were calculated using a potential model developed by Wolf *et al* (1984), in which the interaction potential $V_{ij}(r)$ between two ions i and j has the Born–Mayer–Huggins form:

$$V_{ij}(r) = z_i z_j e^2/r + A_{ij}\exp(-r/\rho_{ij}) - C_{ij}/r^6 \tag{1}$$

where z_i is the charge on ions of type i in units of the electronic charge e. The three terms on the right represent the Coulomb, short-range repulsion, and dispersion energies respectively. This is a standard form of interaction potential for ionic systems. The material is assumed to be fully ionic, with charges of $z_i = 3$, 2, 1 and -2 for Al, Mg, Na and O respectively. The parameters A_{ij}, ρ_{ij} and C_{ij} for the different ion pairs were those derived empirically by Walker and Catlow (1982) from a study of such compounds as Al_2O_3, MgO and Na_2O. This model has been shown to reproduce adequately the important properties of sodium β″-alumina (Wolf *et al* 1984, Zendejas and Thomas 1988).

We have undertaken two sets of simulations, in which x has the values 1/4 and 1/3. The $x = 1/4$ simulations were performed first, using the standard constant-volume

(NVT) MD algorithm, with the volume of the system always the same, and chosen so as to give the values for the lattice parameters quoted above. For the $x = 1/3$ simulations, which were performed later, we used the Parrinello–Rahman constant-pressure (NPT) algorithm (Parrinello and Rahman 1981), with the pressure set equal to zero. The latter algorithm has the advantage that the lattice parameters automatically adjust themselves to yield zero pressure at each temperature. However, we do not believe that the difference of technique affects appreciably the comparisons between the two systems presented later. The Coulombic interactions were treated fully and exactly by the Ewald method. The simulations were run on an Intel iPSC/860 parallel computer employing the replicated data MD algorithm described by Smith (1992). (For technical details of the simulation of ionic materials, see Sangster and Dixon 1976, Gillan 1985, 1990.)

The simulated systems were made as large as practically possible, in order to minimize artificial influences on the formation of the vacancy superlattice. The numbers of sodium, magnesium, aluminium and oxygen ions in the $x = 1/4$ system were 189, 81, 1107 and 1836 respectively; the corresponding numbers for the $x = 1/3$ system were 180, 72, 1116 and 1836. These numbers give 36 complete unit cells in each case, so that each conduction plane has a total of 72 regular sodium sites. Each plane is occupied by 63 sodium ions in the $x = 1/4$ system and 60 sodium ions in the $x = 1/3$ system. Every ion in the system was explicitly treated on an equal footing with every other. The simulations employed the usual periodic boundary conditions. The time step used in integrating the equations of motion was 5×10^{-15} s. The cutoff applied to the short-range potentials (including the real-space part of the Ewald sum) was 5.84 Å in the majority of simulations and 4.86 Å in a small minority.

The simulations for the two different systems followed similar schemes. In both cases the ions were initially placed on the regular lattice sites known from diffraction (Bettman and Peters 1969), with magnesium ions distributed randomly on spinel cation sites, and sodium ions distributed on the hexagonal conduction-plane sites. The lattice parameters were initially set to the crystallographic values. (In the $x = 1/4$ case these remained fixed throughout.) Each system was initialized at high temperature (1200 K for $x = 1/4$ and 1000 K for $x = 1/3$) for a minimum of 20000 time steps (100 ps). Molecular dynamics simulations were performed at several different temperatures ranging from the initialization temperature down to 200 K, with a minimum additional 1000 time steps (5 ps) allowed for equilibration at each temperature. The ion positions at the end of the run for each temperature were used to initiate the simulation at the next lowest temperature. Data were collected at each temperature over intervals of 10000 to 60000 time steps (50 to 300 ps). These long simulations were needed to achieve the required statistical accuracy for the sodium transport properties, particularly at low temperatures.

3. Sodium diffusion

3.1. Mean square displacement

We have studied the sodium diffusion coefficient by examining the time-dependent mean square displacement (MSD) for motion of the sodium ions. This is defined in the usual way as the mean square distance travelled by the ions as a function of time. Since the sodium diffusion is confined within the conduction planes, the motion is highly anisotropic, and we need to distinguish between motion parallel to

and perpendicular to the conduction plane. We denote by $\langle \Delta r_{\parallel}(t)^2 \rangle$ and $\langle \Delta r_{\perp}(t)^2 \rangle$ the mean square displacement of sodium ions in these two directions as a function of time t. For long times, we expect the parallel MSD to obey the relation:

$$\langle \Delta r_{\parallel}(t)^2 \rangle \rightarrow B_{\parallel} + 4D|t| \tag{2}$$

where D is the self-diffusion coefficient parallel to the conduction plane, and $B_{\parallel}$ is a constant. In the perpendicular direction, we expect to find:

$$\langle \Delta r_{\perp}(t)^2 \rangle \rightarrow B_{\perp} \tag{3}$$

where $B_{\perp}$ is a second constant.

We have calculated the MSDs parallel and perpendicular to the conduction plane as an average over all sodium ions and over many time origins, according to the standard methodology (Sangster and Dixon 1976), with time origins taken every 50 steps (0.25 ps) for the $x = 1/3$ simulations and every 25 steps (0.125 ps) for $x = 1/4$. In figure 2, we present plots of $\langle \Delta r_{\parallel}(t)^2 \rangle$ for temperatures of 200, 600 and 1000 K for both the $x = 1/4$ and $x = 1/3$ systems.

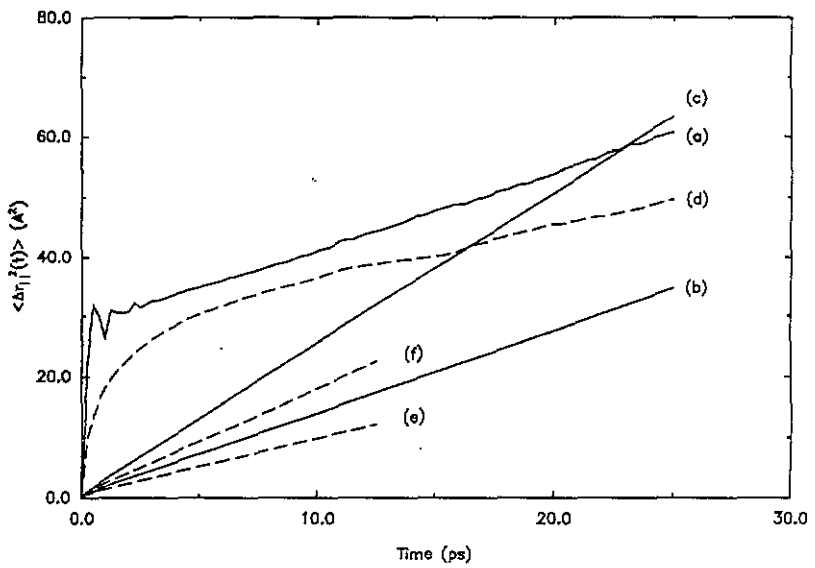

Figure 2. The mean square displacement of sodium ions $\langle \Delta r_{\parallel}(t)^2 \rangle$ parallel to the conduction plane in the simulated systems having compositions $x = 1/3$ (full curves (a)–(c)) and $x = 1/4$ (dashed curves (d)–(f)) at temperatures of 200 K ((a) and (d)), 600 K ((b) and (e)) and 1000 K ((c) and (f)). The results for 200 K are scaled up by factors of 100 for $x = 1/3$ and 50 for $x = 1/4$.

The linearity of the plots provides clear evidence for diffusion in the conduction planes, as expected from previous simulation work (Wolf *et al* 1984, Lane and Farrington 1991). In most cases, the linear region is reached extremely rapidly, typically after a few tenths of a picosecond, in other words a few vibrational periods. This is very similar to what happens in liquids and in many solid electrolytes such as CaF_2 (Gillan 1985, 1990). There is some indication of a departure from this behaviour

in the case of the $x = 1/4$ system at the lowest temperature of 200 K, where the approach to linearity appears to be considerably slower; we return to this matter later.

Plots of our calculated perpendicular MSDs (not shown here) demonstrate that $\langle \Delta r_\perp(t)^2 \rangle$ goes rapidly to a constant value in all cases, which confirms that there is no diffusion along the c-axis, as expected.

3.2. Diffusion coefficient

Equation (2) allows us to obtain the sodium diffusion coefficient D from the slope of $\langle \Delta r_\parallel(t)^2 \rangle$. Our results for D for the two systems are reported in table 1. We draw attention to two points. Firstly, we have been able to calculate values of D over a very wide range of about two orders of magnitude. Secondly, we note that the values of D at the composition $x = 1/3$ are systematically somewhat higher than those at $x = 1/4$ at the higher temperatures. Very roughly, the values stand in the ratio 4:3 which might be expected from the relative concentrations of vacancies. In order to compare our results for D with experiment, we have converted them to the DC electrical conductivity $\sigma(0)$ using the Nernst–Einstein relation (Compaan and Haven 1956):

$$f\sigma(0) = z_{\mathrm{Na}}^2 e^2 \rho_{\mathrm{Na}} D / k_{\mathrm{B}} T \tag{4}$$

where z_{Na}, ρ_{Na} and f are the ionic charge of sodium, the number density of sodium ions and the correlation factor, respectively. The factor f is of order unity, and for the purposes of the semiquantitative comparison we wish to make here we have set it equal to unity.

Table 1. Sodium diffusion coefficient D of simulated β''-alumina at the compositions $x = 1/3$ and $x = 1/4$.

$x = 1/3$		$x = 1/4$	
Temperature (K)	D ($m^2\ s^{-1}$)	Temperature (K)	D ($m^2\ s^{-1}$)
200.0	3.253×10^{-11}	201.2	6.315×10^{-11}
—	—	245.3	1.391×10^{-10}
301.5	3.423×10^{-10}	324.7	3.038×10^{-10}
400.4	1.756×10^{-9}	401.9	9.926×10^{-10}
—	—	501.6	1.849×10^{-9}
600.6	3.373×10^{-9}	624.6	2.340×10^{-9}
805.9	4.940×10^{-9}	801.2	3.898×10^{-9}
997.2	6.325×10^{-9}	1025.1	4.358×10^{-9}
—	—	1195.5	5.318×10^{-9}

In figure 3 we show a comparison of our conductivity results with experimental values on an Arrhenius plot. The following points should be noted. Firstly, we show three sets of experimental results, which come from measurements of Engstrom *et al* (1981) on samples prepared in different ways; we have done this in order to draw attention to the substantial variability of the experimental conductivity at low temperatures. Secondly, we note that the simulation results, like the experimental ones, show a marked change of Arrhenius slope at ~ 400 K, this change being particularly clear for the $x = 1/3$ system. Thirdly, we find that in the high-temperature region

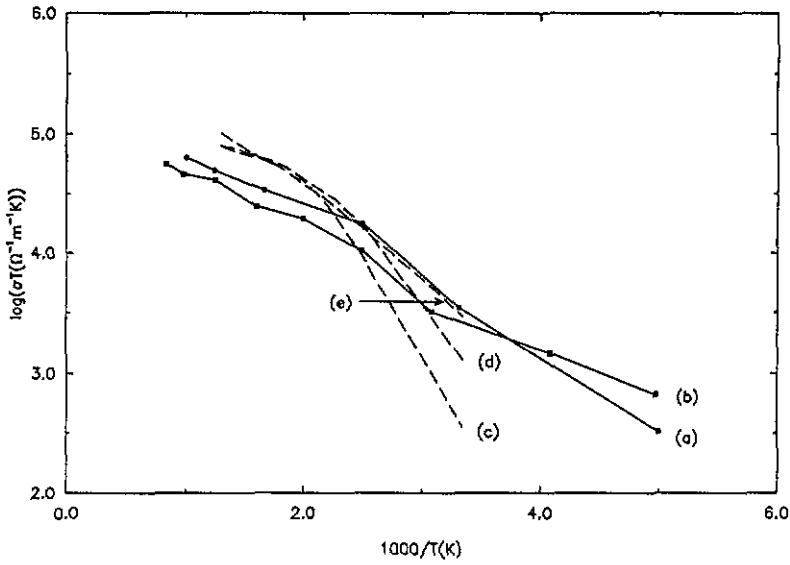

Figure 3. Values of the DC electrical conductivity $\sigma(0)$ obtained from the simulations (dots connected by full lines) at (a) $x = 1/3$ and (b) $x = 1/4$, compared with the experimental results of Engstrom *et al* (1981) (broken curves). The experimental curves are for sodium β''-alumina prepared in different ways: (c) MgO stabilized, grown at 1700 °C; (d) MgO stabilized, grown at 1650 °C; (e) ZnO stabilized, grown at 1700 °C.

the simulation values appear somewhat too low, but our estimated high-temperature activation energies of 0.073 ± 0.003 eV ($x = 1/3$) and 0.085 ± 0.005 eV ($x = 1/4$) compare quite well with experimental values, which lie in the range 0.03–0.09 eV (Briant and Farrington 1980, Engstrom *et al* 1981). Fourthly, the simulation results agree quite satisfactorily with experiment at low temperatures. It should be remarked that since the diffusion coefficient is very small at the lowest temperatures, the calculated values are subject to larger statistical errors in this region.

3.3. Velocity autocorrelation function

Further insight into the dynamics of the sodium ions is gained by examining their velocity autocorrelation function (VACF). As with the MSD, we need to distinguish between VACFs parallel and perpendicular to the conduction plane. The parallel quantity $\zeta_{\parallel}(t)$ is defined as:

$$\zeta_{\parallel}(t) = \langle v_{\parallel}(t) \cdot v_{\parallel}(0) \rangle \tag{5}$$

where $v_{\parallel}(t)$ and $v_{\parallel}(0)$ are the components of the velocity of a given sodium ion parallel to the conduction plane at times separated by t; an analogous definition holds for the perpendicular VACF $\zeta_{\perp}(t)$.

We have calculated the VACFs using standard methods, with time origins taken every 10 steps (0.05 ps) for the $x = 1/4$ system and every 5 steps (0.025 ps) for the $x = 1/3$ system. It is most useful to display the results in the form of the power spectra $z_{\parallel}(\omega)$ and $z_{\perp}(\omega)$, defined as:

$$z_{\parallel}(\omega) = \frac{1}{2} \int_{-\infty}^{\infty} \mathrm{d}t \, \mathrm{e}^{\mathrm{i}\omega t} \zeta_{\parallel}(t) \tag{6}$$

and analogously for $z_\perp(\omega)$.

Our results for $z_\parallel(\omega)$ for the two systems are displayed in figure 4. We note in passing that the value of $z_\parallel(\omega)$ at $\omega = 0$ is just twice the diffusion coefficient D. In fact, this provides an alternative way of calculating D, though in the present calculations it is a less accurate one; we have verified that the values obtained by the two methods give the same results, apart from small statistical differences.

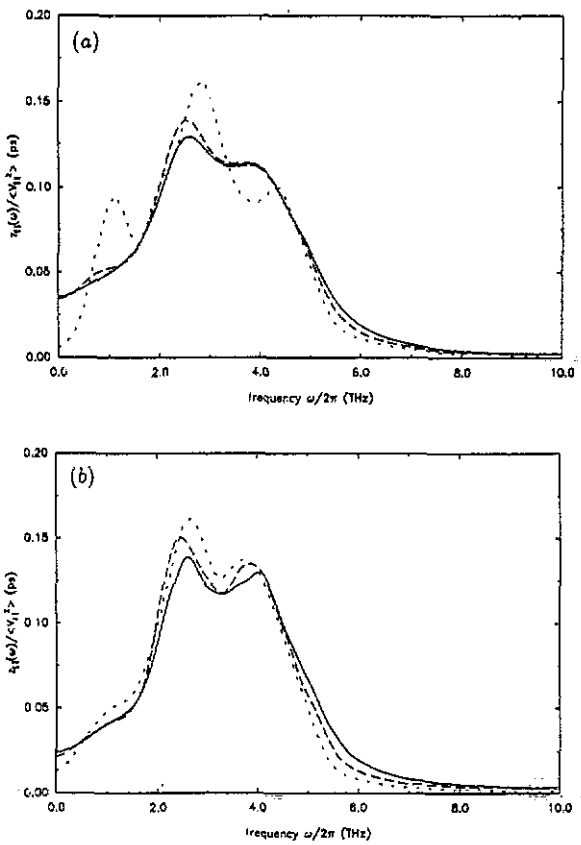

Figure 4. Power spectrum of the normalized VACF $z_\parallel(\omega)/\langle v_\parallel^2\rangle$ of the sodium ions defined as in equation (6). Parts (*a*) and (*b*) of the figure show results for $x = 1/3$ and $x = 1/4$ respectively. Dotted, dashed and full curves give results for temperatures of 200, 600 and 1000 K respectively.

The prominent feature of the spectra is their three-peaked ($x = 1/3$) and two-peaked ($x = 1/4$) structures. The two peaks of higher frequency remain clearly visible up to the highest temperatures, and it is evident that the sodium ions continue to exhibit well defined vibrations about the lattice sites, in spite of their high mobility. The frequencies of the peaks for the $x = 1/3$ system, which at 200 K have values of 1.05, 2.8 and 4.3 THz, can be compared with the frequency-dependent conductivity measurements of Hayes and Hopper (1983) and the Raman data of Dudney *et al* (1983). The Raman spectra show peaks at 0.99, 4.3 and 5.4 THz, which the authors attribute to sodium vibrations; of these, the mode of highest frequency is polarized

along the c-axis, and would not be seen in $z_{\parallel}(\omega)$. The other two frequencies agree rather closely with our simulated values. The structure of the experimental conductivity is more complicated, and shows strong variations with temperature. However, the experimental spectrum at 300 K shows prominent peaks in the region of 1.02, 2.2 and 4.4 THz, though the middle of these peaks shows considerable structure. Again, these frequencies are quite close to our simulated values. It is also noteworthy that the experimental peak at 1.02 THz loses intensity rapidly with increasing temperature, just as in the simulation.

Interestingly, the $x = 1/4$ system does not show a clear peak in the region of 1 THz, though it does exhibit strong dispersion in this region at low temperatures. The effect is closely related to the approach of $\langle \Delta r_{\parallel}(t)^2 \rangle$ to asymptotic linear behaviour at short times: we recall that the rate of approach slows down at low temperatures for $x = 1/4$, but not for $x = 1/3$. The relation between the two effects can be understood in terms of the relation between the MSD and the power spectrum of the VACF:

$$\langle \Delta r_{\parallel}(t)^2 \rangle = B_{\parallel} + 4D|t| - \frac{2}{\pi} \int_{-\infty}^{\infty} d\omega\, \omega^{-2}(z(\omega) - z(0)) \cos \omega t \ . \quad (7)$$

This exact relation, which follows trivially from the definitions of the MSD and the VACF, shows that the difference between $\langle \Delta r_{\parallel}(t)^2 \rangle$ and its asymptotic form is essentially the Fourier transform of the quantity $(z(\omega) - z(0))/\omega^2$. This implies that a slow approach to the asymptotic form must give rise to low-frequency dispersion in $z(\omega)$.

4. The vacancy superlattice

4.1. Formation of the superlattice

It is already fairly well established both from diffraction measurements (Boilot *et al* 1980) and from earlier simulation work (Zendejas and Thomas 1988, Lane and Farrington 1991) that the vacancies become ordered into a superlattice at temperatures below $\sim$ 500 K. The purpose of the present section is to explore the nature of this superlattice through a study of trajectory plots and the radial distribution function.

We have mentioned already that the simulations at higher temperatures were performed first, and that each simulation at a lower temperature was initiated from the final configuration of the preceding one. The main purpose of this procedure was to ensure that the vacancy configurations were completely randomized, and to eliminate all possible bias in the formation of the vacancy superlattice.

To emphasize this point, we show in figure 5(a) a plot of the trajectories of all sodium ions in a chosen conduction plane for the $x = 1/3$ system at 1000 K; the trajectories are shown for a time span of 5000 time steps (25 ps). The extremely rapid diffusion of the ions expected from the high value of the diffusion coefficient at this temperature is evident. It is also clear that diffusion occurs by movement of the ions directly between nearest-neighbour sites on the hexagonal lattice. We note that even at this high temperature strong concentrations of density are localized on the regular sites. This is consistent with the model of discrete inter-site jumps proposed by previous workers. The diffusion dynamics becomes clearer if one examines the trajectories of individual ions. Figure 5(b) shows the trajectories over a period of 25 ps of four ions chosen at random from the same simulation at 1000 K. It is clear

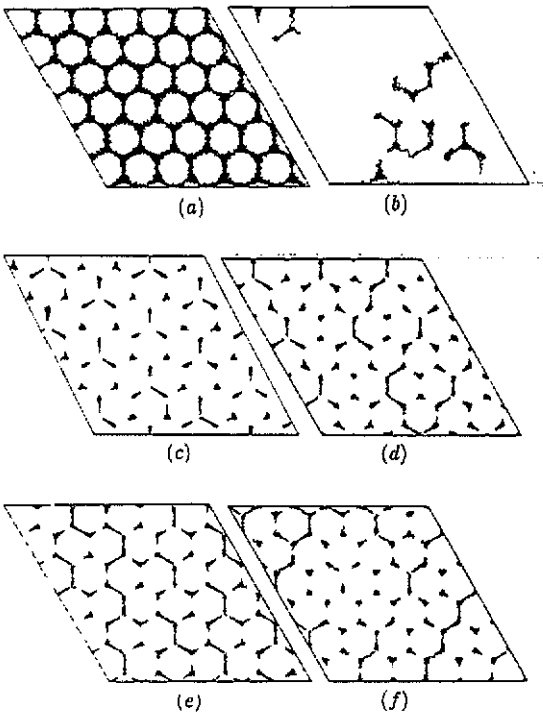

Figure 5. Trajectory plots of sodium ions in a conduction plane over a time window of 25 ps: (*a*) $x = 1/3$ system at 1000 K; (*b*) same as (*a*) but showing only selected ions; (*c*) $x = 1/3$ system at 200 K; (*d*) $x = 1/4$ system at 200 K; (*e*) $x = 1/3$ system at 200 K; (*f*) $x = 1/4$ system at 200 K.

from this that each ion undertakes roughly four diffusive jumps in this time span. A simple estimate shows that this is what would be expected. If ν denotes the rate at which an ion jumps from an initial site to any of the neighbouring sites, and the intersite distance is d_0, then assuming successive jumps to be uncorrelated we would have $D = \frac{1}{4}d_0^2\nu$. From the value of D reported in the previous section, we obtain the estimate $\nu = 0.24 \times 10^{12}\ s^{-1}$, so that the residence time of the ions is 4.1 ps, which is roughly consistent with what the trajectory plots reveal. For the $x = 1/3$ system, there is one vacancy for every 6 ions, so that the residence time of the vacancies is roughly 0.69 ps. Since the duration of the simulation at each temperature is typically 100 ps or more, it is clear that any possible bias in the vacancy distribution must have been completely eliminated by the time we arrive at lower temperatures.

We now show typical plots for the $x = 1/3$ and $x = 1/4$ systems obtained at 200 K (figures 5(*c*) and (*d*) respectively); the time span is 25 ps, as in the previous plots. The characteristics of the trajectories are, of course, radically different from those observed at high temperatures. We note that intersite jumps are extremely infrequent. This is expected, since the diffusion coefficient at 200 K is roughly two orders of magnitude less than its value at 1000 K. The simple calculation outlined above gives estimates of 135 ps and 52.0 ps for the residence times of the vacancies at 200 K in the $x = 1/3$ and $x = 1/4$ systems, which are consistent with what we observe in the trajectory plots. There are a number of other remarkable features. Firstly, we note the clear visibility of the vacancies. It has been known for some years from

diffraction work (Roth *et al* 1973, Boilot *et al* 1980) and from MD simulations (Wolf *et al* 1984) that vacancies in β″-alumina induce a strong inward relaxation of the three neighbouring sodium ions. This gives rise to the characteristic triad structures visible in the plots. Secondly, it is clear in both the $x = 1/4$ and the $x = 1/3$ systems that the vacancies are ordered into a superlattice, but that the superlattice has a completely different symmetry in the two cases. For the $x = 1/3$ system (figure 5(*c*)), the translation vectors of the superlattice are $a(3/2, \sqrt{3}/2)$ and $a(0, \sqrt{3})$ which is exactly what has been deduced from the diffuse scattering measurements of Boilot *et al* (1980). (Note that the material studied by those authors has a composition close to $x = 1/3$.) The $x = 1/4$ system, by contrast (figure 5(*d*)), has a superlattice with translation vectors $a(2, 0)$ and $a(1, \sqrt{3})$.

It should be added here that since there is a measurable diffusion coefficient even at 200 K, some disorder in the superlattice must exist. This is already apparent in figure 5(*d*), and is illustrated more clearly in figures 5(*e*) and (*f*) which show further trajectory plots for the $x = 1/3$ and $x = 1/4$ systems at 200 K.

4.2. The radial distribution function

Further information about the spatial distribution of the ions can be obtained from the radial distribution function (RDF) for the sodium ions.

Figures 6(*a*) and (*b*) show the sodium–sodium RDFs for the two systems at temperatures of 200 K and 800 K. As expected, there is a marked loss of structure as we go from low to high temperatures. More interesting than this is the appreciable weakening of structure as we go from $x = 1/4$ to $x = 1/3$: both at low and at high temperatures, the first peak of the distribution is substantially broader in the system having the higher concentration of vacancies. The strong difference between the two systems is also apparent in the remarkable shift of the radial position of the first peak. Finally, we note that at low temperatures a subsidiary peak is visible in the RDF at a radius of ~ 4.5 Å. There is a close relation between this subsidiary peak and the shift of the first peak, as we now show.

The subsidiary peak has been observed in previous simulation work on β″-alumina, and has been attributed to the correlation between relaxed ions neighbouring the vacancies (Wolf *et al* 1984). Our results fully support this interpretation. If we suppose that each of the three ions surrounding a vacancy relaxes towards the vacancy by a distance ya, where a, as before, is the lattice parameter, then the distance between these relaxed ions is easily shown to be $d_2 = a(1 - \sqrt{3}y)$. Taking the radius of the subsidiary peak to be 4.5 Å, this implies a relaxational displacement $ya = 0.67$ Å, which is close to the value of 0.8 Å deduced from diffraction measurements (Roth *et al* 1973, 1979, Boilot *et al* 1980).

Now consider the first peak, which must evidently consist of correlations between unrelaxed ions that are not vacancy neighbours, and between these unrelaxed ions and relaxed ions that are vacancy neighbours. The distance d_0 between unrelaxed ions, i.e. the separation of neighbouring sites on the hexagonal lattice, is $a/\sqrt{3}$, and the distance d_1 between a relaxed ion and the nearest unrelaxed ions is $a(1/3 + y/\sqrt{3} + y^2)^{1/2}$. We expect the radius of the first peak to be a weighted average of d_0 and d_1. In the $x = 1/3$ system, for the case that the vacancy superlattice is perfectly ordered, it is readily shown that *all* the neighbours of an unrelaxed ion are relaxed neighbours of a vacancy, and we therefore expect the first peak to fall at the radius d_1. From the low temperature RDF of figure 6(*a*), we estimate this radius to

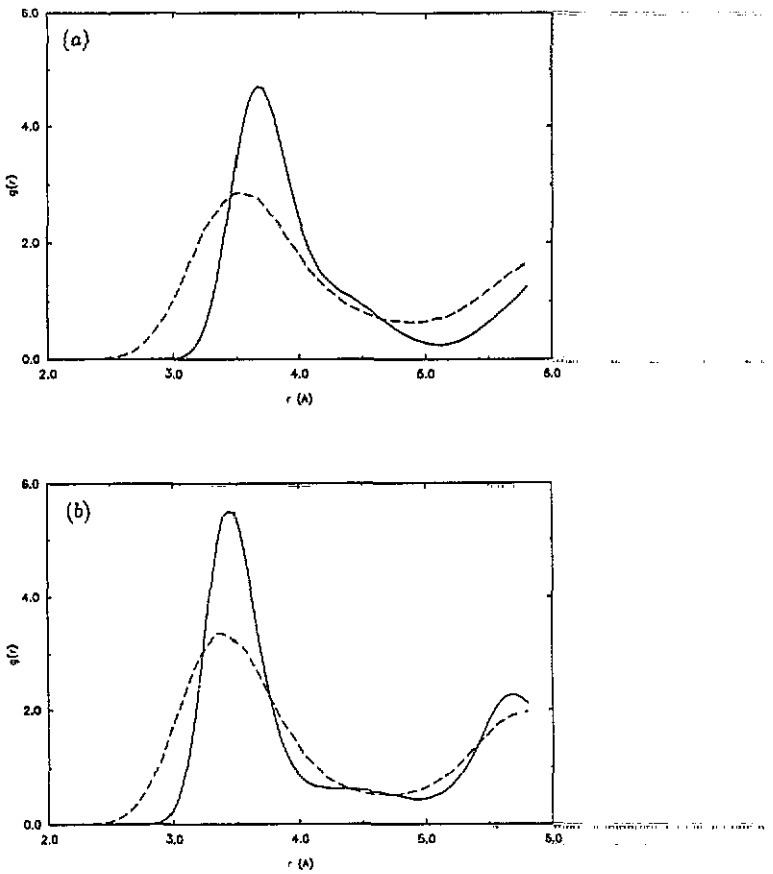

Figure 6. The sodium–sodium radial distribution function $g(r)$ calculated from the simulations at 200 K (full curve) and 800 K (dashed curve). Panels (*a*) and (*b*) show results for $x = 1/3$ and $x = 1/4$ respectively.

be 3.67 Å, which yields the result $ya = 0.73$ Å, in close agreement with the estimate based on the position of the subsidiary peak. On the other hand, for the $x = 1/4$ system, with perfect vacancy ordering, we find that 1/3 of nearest-neighbour distances will be d_0 and 2/3 will be d_1. With $d_0 = 3.24$ Å and $d_1 = 3.67$ Å, we predict the peak position to be 3.49 Å, which is in excellent accord with what we observe (figure 6(*b*)).

At high temperatures, when the vacancy superlattice breaks down and the vacancy distribution becomes more random, we would expect the peak position to shift to lower values, which again is what we observe.

The conclusion from these results is that the features of the RDFs reveal both the internal structure of the vacancies and the characteristics of vacancy ordering at low temperatures.

5. The structure factor

The ordering of vacancies at low temperatures in β''-alumina was first proposed because of the observation of diffuse x-ray scattering at characteristic wavevectors (Boilot

Table 2. Values of the structure factor of simulated β″-alumina with compositions $x=1/4$ and $x=1/3$ at temperatures of 200 and 1000 K, at reciprocal lattice vectors G satisfying equation (13). The tabulated quantity is $N^{-1}S(G)$. The G vectors are specified through the indices h, k and l (see equation (13)).

			$x = 1/3$		$x = 1/4$	
h	k	l	200 K	1000 K	200 K	1000 K
0	0	3	0.995	0.989	0.994	0.986
0	0	6	0.982	0.956	0.975	0.946
0	1	−4	0.160	0.156	0.159	0.154
0	1	−1	0.191	0.181	0.196	0.181
0	1	2	0.223	0.203	0.234	0.205
0	1	5	0.255	0.222	0.271	0.225
1	−1	−4	0.153	0.151	0.160	0.152
1	−1	−1	0.183	0.176	0.197	0.179
1	−1	2	0.214	0.198	0.235	0.203
1	−1	5	0.245	0.216	0.273	0.223
1	0	−5	0.262	0.216	0.273	0.226
1	0	−2	0.229	0.198	0.235	0.207
1	0	1	0.196	0.176	0.197	0.182
1	0	4	0.164	0.151	0.160	0.155
1	1	−6	0.398	0.282	0.482	0.319
1	1	−3	0.404	0.292	0.492	0.332
1	1	0	0.405	0.296	0.495	0.337
1	1	3	0.403	0.293	0.491	0.332
1	1	6	0.396	0.283	0.480	0.318

et al 1980). It is therefore of great interest to know whether we can detect diffuse intensity in the structure factor of the simulated system. Another reason for studying the structure factor is that it will give us a quantitative measure of the strength of vacancy correlations. Although the trajectory plots presented in the previous section provide convincing qualitative evidence for vacancy ordering in the simulated systems, the structure factor will provide us with sound quantitative information.

5.1. *Bragg peaks*

The object of interest here is the structure factor $S(\boldsymbol{k})$ describing correlations between sodium ions, which we define as

$$S(\boldsymbol{k}) = \langle |\hat{\rho}_{\boldsymbol{k}}|^2 \rangle \tag{8}$$

where $\hat{\rho}_{\boldsymbol{k}}$ is the density of sodium ions at wavevector $\boldsymbol{k}$, given by

$$\hat{\rho}_{\boldsymbol{k}} = N^{-1/2} \sum_{j=1}^{N} \exp(\mathrm{i}\boldsymbol{k} \cdot \boldsymbol{r}_j) \tag{9}$$

and $\langle \ldots \rangle$ represents the average in thermal equilibrium. In the definition of $\hat{\rho}_{\boldsymbol{k}}$, the sum goes over the N sodium ions in the system, and $\boldsymbol{r}_j$ is the time-varying position of the jth ion. With the normalization we have adopted, the maximum value of $S(\boldsymbol{k})$, which is attained at $\boldsymbol{k} = 0$, is N. It should be noted that in the simulations, $S(\boldsymbol{k})$ can be calculated only for those $\boldsymbol{k}$ that are compatible with the periodic boundary conditions, namely the reciprocal lattice vectors associated with the simulation itself.

We have calculated the structure factor for a wide range of wavevectors and for the full range of temperatures studied in this work. In presenting the results, it is useful to deal first with the reciprocal lattice vectors of the perfect crystal, where we expect to find Bragg peaks in the structure factor. The primitive translation vectors a_i of the perfect stoichiometric crystal are, in cartesian components:

$$a_1 = a(1,0,0) \qquad a_2 = a(-1/2, \sqrt{3}/2, 0) \qquad a_3 = c(0,0,1) \quad (10)$$

where a and c are the lattice parameters to which we have already referred. The primitive reciprocal lattice vectors b_i ($a_i \cdot b_j = 2\pi\delta_{ij}$) are given by:

$$b_1 = \frac{2\pi}{a}(1, 1/\sqrt{3}, 0) \qquad b_2 = \frac{2\pi}{a}(0, 2/\sqrt{3}, 0) \qquad b_3 = \frac{2\pi}{c}(0,0,1). \quad (11)$$

The general reciprocal lattice vector G is:

$$G = hb_1 + kb_2 + lb_3 \quad (12)$$

with h, k and l integers. The threefold screw symmetry leads to missing orders in diffraction, and it is readily shown that the structure factor for the perfect crystal is only non-zero for G vectors satisfying the condition:

$$-h + k + l = 3n \quad (13)$$

where n is an integer. For G vectors satisfying this condition, $N^{-1}S(G)$ is equal to unity in the perfect stoichiometric crystal. In the defective crystal in thermal equilibrium, it will be reduced below this value by vibrational and vacancy-induced disorder.

In table 2 we give the calculated structure factors for reciprocal lattice vectors G satisfying equation (13) for the $x = 1/4$ and $x = 1/3$ systems at low and high temperatures. As expected, $N^{-1}S(G)$ decreases with increasing temperature, vacancy concentration and wavevector. For reciprocal lattice vectors not satisfying equation (13), we find that $S(G)$ is smaller than the values given in table 3 by at least two orders of magnitude.

5.2. *Diffuse peaks*

Turning now to the diffuse intensity, we note first that the vacancy correlations that interest us are expected to be entirely *within* the conduction planes: because of the large distance between the planes, correlations between different planes are expected to be negligible. This means that for k that are not reciprocal lattice vectors the associated $S(k)$ should be almost independent of the component $k_\perp$ of k perpendicular to the conduction plane, except for very large $k_\perp$. We therefore present the results in terms of an average $\bar{S}(k_\parallel)$ over the wavevector component $k_\perp$, with $k_\parallel$ the component of wavevector parallel to the conduction plane. In the results to be presented here, the average is taken over values of $k_\perp$ ranging from $-12\pi/c$ to $12\pi/c$.

Figure 7 displays our results for the averaged intensity $\bar{S}(k_\parallel)$ as a function of the two-dimensional wavevector $k_\parallel$ for the $x = 1/4$ and $x = 1/3$ systems at temperatures of 200, 300 and 400 K. Because of the periodic boundary conditions, we can only

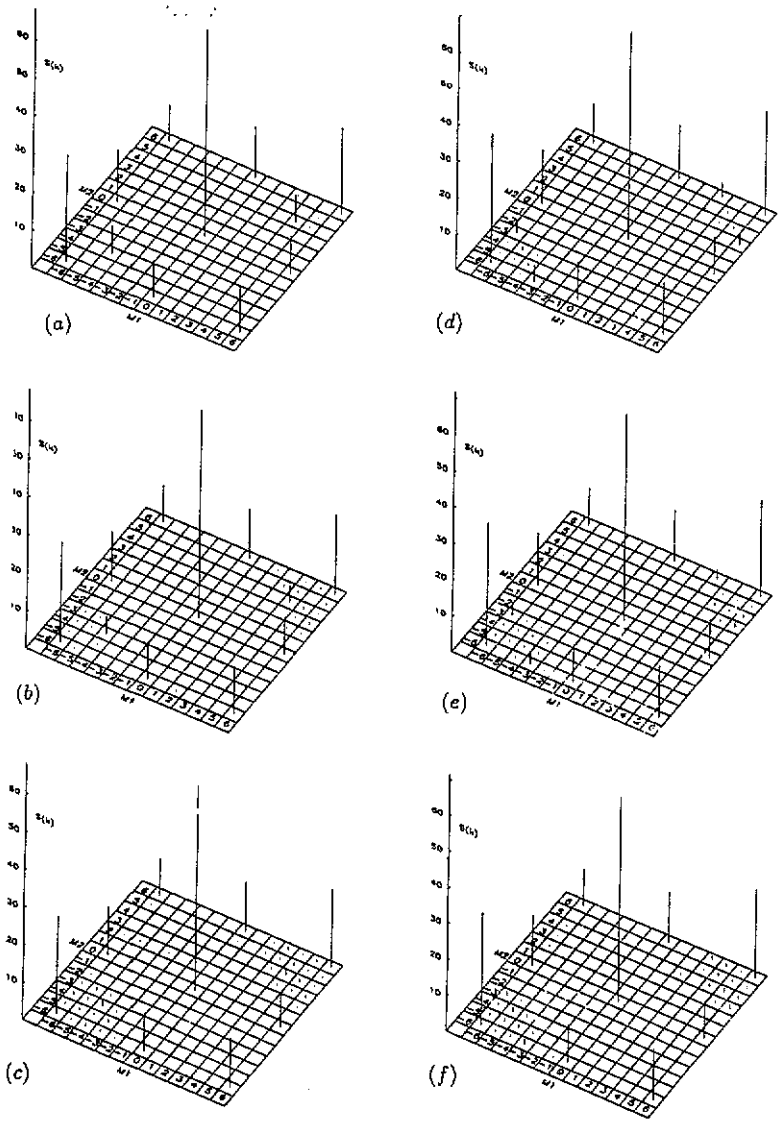

Figure 7. Structure factors $\tilde{S}(\boldsymbol{k}_{\|})$ of the simulated system, averaged over the component $k_{\perp}$ of wavevector perpendicular to the conduction plane. Panels (*a*)–(*c*) show results for the $x = 1/3$ system at temperatures of 200, 300 and 400 K respectively, and panels (*d*)–(*f*) show results for $x = 1/4$ at the same three temperatures. Values of $\tilde{S}(\boldsymbol{k}_{\|})$ are given on the two-dimensional grid of wavevectors $\boldsymbol{k}_{\|}$ that are compatible with the periodic boundary conditions, with $\boldsymbol{k}_{\|}$ specified by integers M_1 and M_2 according to the formula $\boldsymbol{k}_{\|} = (M_1\boldsymbol{b}_1 + M_2\boldsymbol{b}_2)/6$.

examine wavevectors $\boldsymbol{k}_{\|}$ having the form $(M_1\boldsymbol{b}_1 + M_2\boldsymbol{b}_2)/6$, where M_1 and M_2 are integers; the divisor 6 comes from the fact that the primitive translation vectors of the simulation supercell parallel to the conduction plane are $6\boldsymbol{a}_1$ and $6\boldsymbol{a}_2$. The figure shows as vertical lines the intensities for all $\boldsymbol{k}_{\|}$ having $-6 \leqslant M_i \leqslant 6$. It should be noted that the largest intensities occur when M_1 and M_2 are *both* divisible by 6; these are reciprocal lattice vectors of the crystal, and the intensities at these points

are the Bragg peaks discussed in section 5.1. Diffuse intensity occurs at other values of M_i.

Prominent diffuse peaks are visible at 200 K, which weaken rapidly with increasing temperature. In the $x = 1/4$ system, these peaks occur at $(M_1, M_2) = (6, 3), (3, 6), (-6, -3)$ and $(-3, -6)$ corresponding to the wavevector $k_\parallel = b_1 + \frac{1}{2}b_2$ and other wavevectors in the same star. In the $x = 1/3$ system, they occur at $(M_1, M_2) = (4, 4)$ and $(-4, -4)$ corresponding to the star of wavectors represented by $k_\parallel = \frac{2}{3}(b_1 + b_2)$.

It is readily shown that these wavevectors are reciprocal lattice vectors of the vacancy superlattices in the two systems. In the $x = 1/4$ case, it is clear from figure 5(d) that the primitive translation vectors of the superlattice parallel to the conduction plane are:

$$A_1 = 2a_1 \qquad A_2 = 2a_2 \tag{14}$$

so that the primitive reciprocal lattice vectors are

$$B_1 = \tfrac{1}{2}b_1 \qquad B_2 = \tfrac{1}{2}b_2. \tag{15}$$

It follows that the general reciprocal lattice vectors of the superlattice are:

$$k_\parallel = n_1B_1 + n_2B_2 = \tfrac{1}{2}(n_1b_1 + n_2b_2). \tag{16}$$

The wavevectors in the star of $b_1 + \frac{1}{2}b_2$ are among these. In the case of $x = 1/3$, the primitive translation vectors of the superlattice are:

$$A_1 = 2a_1 + a_2 \qquad A_2 = a_1 + 2a_2 \tag{17}$$

so that the primitive reciprocal lattice vectors are:

$$B_1 = \tfrac{2}{3}b_1 - \tfrac{1}{3}b_2 \qquad B_2 = -\tfrac{1}{3}b_1 + \tfrac{2}{3}b_2. \tag{18}$$

It follows from this that the general reciprocal lattice vectors are:

$$k_\parallel = n_1b_1 + n_2b_2 + \beta \tag{19}$$

where

$$\beta = 0, \pm\tfrac{1}{3}(b_1 + b_2)\,. \tag{20}$$

The wavevectors in the star of $\frac{2}{3}(b_1 + b_2)$ are among these.

In both cases, then, the peaks of diffuse intensity lie at reciprocal lattice vectors of the vacancy superlattice, and it seems certain that the vacancy correlations are directly responsible for the diffuse intensity. This conclusion is reinforced by further considerations given in the Appendix. We show there that simple estimates can be given for the expected diffuse intensity, and that these estimates explain why intensity is not observed at all reciprocal lattice vectors of the superlattice.

Finally, we show results for the temperature dependence of the diffuse intensity. Figure 8 displays the average intensity $\bar{S}(k_\parallel)$ for the $x = 1/4$ and $x = 1/3$ systems at the wavevectors $k_\parallel = b_1 + \frac{1}{2}b_2$ and $\frac{2}{3}(b_1 + b_2)$ respectively, where the intensity is greatest. It is clear from this that the intensity falls off very rapidly with increasing temperature, becoming essentially zero above 400 K. This is in complete accord with the x-ray studies of Boilot *et al* (1980), which show the rapid broadening of diffuse intensity in reciprocal space in this temperature range. We shall comment in the following section on the fact that this is also the temperature range in which the Arrhenius slope of the conductivity shows a marked change.

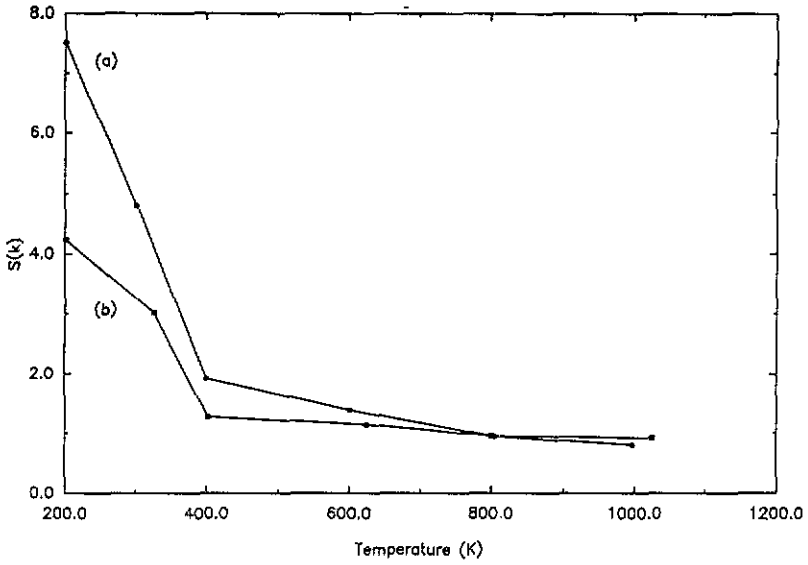

Figure 8. Temperature dependence of $\bar{S}(k_{\|})$ for sodium diffuse scattering peaks: (*a*) $x = 1/3$ system, in the star of wavevectors $k_{\|} = b_1 + \frac{1}{2}b_2$; (*b*) $x = 1/4$ system, in the star of wavevectors $k_{\|} = \frac{2}{3}(b_1 + b_2)$.

6. Discussion

This work has yielded three important achievements. Firstly, we have shown that MD simulation of sodium β″-alumina reproduces the non-Arrhenius behaviour of the electrical conductivity that is known from experiment. Secondly, we have been able to observe the spontaneous formation of the vacancy superlattice at low temperatures, and to follow the breakdown of this superlattice with increasing temperature. Thirdly, we have shown how the symmetry of the superlattice depends crucially on the vacancy concentration. We stress that the ability to perform long simulations on large systems has played an essential role in the work. The large size of the system is important because it reduces any artificial influence of the periodic boundary conditions on vacancy ordering; the long duration of the simulations is needed in order to obtain the statistical accuracy required to study the diffusion coefficient at low temperatures. We now comment further on these points.

Our results for the electrical conductivity agree semiquantitatively with experiment over the temperature range we have examined. In judging this comparison (figure 3), it should be borne in mind that we have set the correlation factor f in the Nernst–Einstein relation equal to unity. In fact, f will be somewhat less than unity, so that the agreement at high temperatures is probably better than it might appear. The significant feature is that our high-temperature activation energy is quite close to the experimental value. The marked change of activation energy that we find at 400 K is entirely clear for $x = 1/3$, which is the composition normally observed, and somewhat less so at $x = 1/4$. It should be noted here that at our lowest temperature of 200 K, our values for the conductivity are subject to sizable statistical errors, even with the long runs we have employed.

Turning now to the vacancy superlattice, we note first the importance of the two complementary methods of study we have used. The inspection of trajectories in

real space gives the most direct and intuitive means of observing the superlattice. However, this method is unsystematic, and gives no means of assessing the degree of spatial ordering of the vacancies. The quantitative information that we need is supplied by our study of the sodium structure factor. Both methods show clearly that the symmetry of the superlattice depends crucially on the vacancy concentration. In fact, for the two concentrations that we have studied, the symmetry is determined entirely by geometry: the symmetry adopted is the one required to ensure that every superlattice site is occupied by a vacancy.

Our structure-factor results have shown that the degree of spatial ordering of the vacancies is strongly dependent on temperature. For both the $x = 1/4$ and $x = 1/3$ systems, the structure factor shows prominent diffuse peaks at 200 K, but these become almost unobservable above about 400 K. In the diffuse-scattering experiments of Boilot *et al* (1980), the quantity reported is the 'coherence length' of the superlattice (i.e. the distance over which the vacancies are correlated), which is related to the width of the diffuse peaks in wavevector space. Unfortunately, this width cannot be directly seen in our simulations, since the periodic boundary conditions restrict our wavevector resolution too much. However, the strong reduction of the coherence length observed by Boilot *et al* (1980) at about 500 K corresponds fairly closely to the loss of correlation in this temperature range revealed in our simulations.

Finally, we point to some questions that are left unresolved by the present work. The first concerns the relation between the non-Arrhenius behaviour of conductivity and the formation of the vacancy superlattice. It has been suggested that 'pinning' of vacancies by the superlattice may be responsible for deviations from Arrhenius behaviour at low temperatures (Boilot *et al* 1980, Wang *et al* 1981, Bates *et al* 1981). The present simulations open the way to the study of the relation between the two effects, which we hope to undertake in the future. A second, related question concerns the dynamics of the superlattice. Even at low temperature, the vacancy superlattice cannot be completely regular, because we know that the vacancies must diffuse. This implies that the superlattice must be in a state of continual breakdown and renewal. The dynamics of this process remain at present completely obscure. It seems likely that future molecular dynamics work will also be able to shed light on this question.

Acknowledgments

We are grateful to the Daresbury Advanced Research Computing Group for a generous allocation of time on the Intel iPSC/860. We also thank Professor Richard Catlow for his encouragement and advice in the early stages of this work.

Appendix. Diffuse scattering from correlated vacancies

We have shown that the vacancy superlattice gives rise to diffuse peaks in the sodium structure factor, but that these peaks are observable only at some of the reciprocal lattice vectors of the superlattice. The purpose of this Appendix is to explain briefly how this comes about. Other aspects of diffuse scattering from vacancy systems have been discussed previously by Gillan and Wolf (1985) and Gillan (1986).

The structure factor $S(k)$ is a measure of the intensity of fluctuations of the density $\hat{\rho}_k$ at wavevector k. We consider $\hat{\rho}_k$ first for a system containing a single

vacancy. This is given by:

$$\hat{\rho}_k = N^{-1/2} {\sum_j}' e^{ik \cdot R'_j} \tag{21}$$

where j goes over sites other than the vacancy site, and R'_j is the relaxed position of the sodium ion at site j; the prime on the summation indicates omission of the vacancy site itself. For k not equal to a reciprocal lattice vector, $\hat{\rho}_k$ for the perfect crystal is zero, so we can write the density in the vacancy system equivalently as:

$$\hat{\rho}_k = N^{-1/2}\left({\sum_j}' e^{ik \cdot R'_j} - \sum_j e^{ik \cdot R_j} \right) \tag{22}$$

where R_j are the positions in the perfect lattice. When we make rough estimates below, we shall include only relaxation of the three nearest neighbours, so that terms in this equation for more distant neighbours cancel, and we get:

$$\hat{\rho}_k = N^{-1/2}[e^{ik \cdot R'_1} + e^{ik \cdot R'_2} + e^{ik \cdot R'_3} - e^{ik \cdot R_1} - e^{ik \cdot R_2} - e^{ik \cdot R_3} - 1] \tag{23}$$

where $j = 1, 2, 3$ represents the three neighbours, and it is assumed that the position of the vacancy is at $R_0 = 0$. We shall use the notation $\hat{\rho}_k = N^{-1/2}\hat{\sigma}_k$, where $\hat{\sigma}_k$ is the quantity in square brackets in equation (23).

If now we have ν vacancies, whose positions are R_I, the density is:

$$\hat{\rho}_k = N^{-1/2}\hat{\sigma}_k \sum_{I=1}^{\nu} e^{ik \cdot R_I} \,. \tag{24}$$

In terms of these quantities, the structure factor (see equations (8) and (9)) is:

$$S(k) = |\hat{\sigma}_k|^2 N^{-1} \left\langle \sum_{I,J} \exp[ik \cdot (R_I - R_J)] \right\rangle \,. \tag{25}$$

This means that the structure factor is a product of two factors, the first of which, namely $|\hat{\sigma}_k|^2$, represents the intrinsic structure of the vacancies, and the second of which represents correlations *between* vacancies. If there was only the second factor, there would be diffuse peaks at all reciprocal lattice vectors of the superlattice; in reality, the intensity of these peaks is strongly modulated by the first factor.

We now illustrate how this works for particular wavevectors. For the $x = 1/3$ system, the wavevector $k_{\|} = \frac{1}{3}(b_1 + b_2)$ is a reciprocal lattice vector of the superlattice, though no significant diffuse intensity is found there. For this $k_{\|}$, it is readily shown from equation (23) that

$$\hat{\sigma}_k = 2\cos\left[\frac{2\pi}{3}(1 - \sqrt{3}y)\right] \tag{26}$$

where ya is the inward displacement of neighbours, as in section 4.2. Taking $ya = 0.67$ Å from the results of that section, we find $\hat{\sigma}_k = 0.18$, so that the factor $|\hat{\sigma}_k|^2$ in

equation (25) has the very small value of 0.03. On the other hand, for the wavevector $k_{\|} = \frac{2}{3}(b_1 + b_2)$, we find

$$\hat{\sigma}_k = 2\cos\left[\frac{4\pi}{3}(1 - \sqrt{3}y)\right] \tag{27}$$

whose numerical value is 1.97, so that $|\hat{\sigma}_k|^2 = 3.87$. This means that the structure factor arising from vacancy correlations at the second of these wavevectors has roughly 100 times the value that it does at the first. This explains why we find diffuse intensity at the second and not the first wavevector. Similar estimates at other wavevectors can be shown to account completely for our structure-factor results.

References

Bates J B and Farrington G C (ed) 1981 *Proc. Int. Conf. on Fast Ionic Transport in Solids (Gatlinburg, 1981)* (Amsterdam: North-Holland)

Bates J B, Engstrom H, Wang J C, Larson B C, Dudney N J and Brundage W E 1981 *Solid State Ionics* **5** 159

Bettman M and Peters C R 1969 *J. Phys. Chem.* **73** 1774

Boilot J P, Collin G, Colomban P and Comes R *1980 Phys. Rev.* **22** 5912

Briant J L and Farrington G C 1980 *J. Solid State Chem.* **33** 385

Compaan K and Haven Y 1956 *Trans. Faraday Soc.* **52** 786

Dudney N J, Bates J B and Brundage W E 1983 *Solid State Ionics* **9–10** 207

Engstrom H, Bates J B, Brundage W E and Wang J C 1981 *Solid State Ionics* **2** 265

Farrington G C and Briant J L 1979 *Science* **204** 1371

Gillan M J 1985 *Physica* **131B** 157

—— 1986 *J. Phys. C: Solid State Phys.* **19** 3391

—— 1990 in *Ionic Materials at High Temperatures* ed A M Stoneham (London: World Scientific) p 169

Gillan M J and Wolf D 1985 *Phys. Rev. Lett.* **55** 1299

Hayes W and Hopper G F 1983 *J. Phys. C: Solid State Phys.* **16** 2529

Kleitz M, Sapoval B and Chabre Y (ed) 1983 *Proc. Int. Conf. on Solid State Ionics (Grenoble, 1983)* (Amsterdam: North-Holland)

Lane C and Farrington G C 1991 preprint

Parrinello M and Rahman A 1981 *J. Appl. Phys.* **52** 7182

Roth W L, Hamilton W C and LaPlaca S J 1973 *Am. Cryst. Assoc. Abstr. Ser.2* **1** 169

Roth W L, Anne M, Tranqui D and Heidemann A 1979 *Fast Ion Transport in Solids* ed P Vashishta, J N Mundy and G K Shenoy (Amsterdam: North-Holland) p 527

Sangster M J L and Dixon M 1976 *Adv. Phys.* **25** 247

Smith W 1992 *Comput. Phys. Commun.* **67** 392

Smith W and Gillan M J 1991 *Ber. Bunsenges. Phys. Chem.* **95** 967

Walker J R and Catlow C R A 1982 *J. Phys. C: Solid State Phys.* **15** 6151

Wang J C, Bates J B, Dudney N J and Engstrom H 1981 *Solid State Ionics* **5** 35

Weppner W and Schulz H (ed) 1988 *Proc. 6th Int. Conf. on Solid State Ionics (Garmisch-Partenkirchen, 1988)* (Amsterdam: North-Holland)

Wolf M L, Walker J R and Catlow C R A 1984 *Solid State Ionics* **13** 33

Zendejas M A and Thomas J O 1988 *Solid State Ionics* **28–30** 46